DE GRUYTER OPEN GOSPODARKA SUROWCAMI MINERALNYMI – MINERAL RESOURCES MANAGEMENT
2015 Volume 31 Issue 4 Pages 51–74
DOI 10.1515/gospo-2015-0038

SOMAYEH REZAEI*, MOHAMMAD LOTFI*, PEYMAN AFZAL**,
MOHAMMAD REZA JAFARI*, MOJTABA SHAMSEDDIN MEIGOONY***,
MASOUMEH KHALAJMASOUMI***

Investigation of copper and gold prospects using index overlay integration method and multifractal modeling in Saveh 1:100,000 sheet, Central Iran

Introduction

Mineral deposit formation is one of complicated geological processes in which multiple factors affect their formation and appearance. In order to prospect the mineral potential areas, comprehensive studies of geological layers, remote sensing and geophysics seem essential to determine the interrelationships of effective factors in mineralization. Therefore GIS is influential in recognition of probable potential areas by collecting, processing, exploration layered weighing and integrating thematic maps (Noorollahi et al. 2008; Yousefifar et al. 2011). The selection of the prospect areas in mineral exploration is a complex process and needs various criteria (Carranza 2008; Pazand et al. 2014). As there is no certainty in various geological phenomena, diverse methods of modeling and combination of information layers such as Boolean Operation, Index Overlay, Analytical Hierarchy Process (AHP),

* Department of Geology, North Tehran Branch, Islamic Azad University, Tehran, Iran;
e-mail: somaiehrezaei@yahoo.com
** Department of Mining Engineering, South Tehran Branch, Faculty of Engineering,
Islamic Azad University, Tehran, Iran; Camborne School of Mines, University of Exeter, Penryn, UK.
*** Department of Geology, Science and Research Branch, Islamic Azad University, Tehran, Iran.

Fuzzy Logic and Genetic Algorithm are used to obtain proper results for determination of ore prospects (Bonham-Carter 1991, 1994; Carranza 2008; Harris 1989; Karimi and Valadan Zoej 2004; Malczewski 2006; Moradi et al. 2014; Pazand et al. 2011; Porwal et al. 2003; 2006; Yousefifar et al. 2011).

Fractal geometry established by Mandelbrot (1983), is an important branch of nonlinear mathematics and has been used in different geological fields since 1980s. The fractal/multifractal modeling applies for classification of different characteristics in geosciences (Afzal et al. 2012, 2013; Agterberg 1995; Cheng and Agterberg 2009; Sim et al. 1999; Zuo 2011). Using all data without modifying them, considering data spatial distribution, geometrical shape of various areas concerning the distribution of the studied parameter are fundamental advantages of these methods (Afzal et al. 2010, 2014; Cheng et al. 1994; Cheng 1999; Davis 2002; Li et al. 2003; Zuo et al. 2009, 2013).

In this paper, index overlay as one of common methods of integrating different layers was used in Saveh 1 : 100,000 sheet, Central Iran. Due to the fact that in this method each layer has different classes, it takes priority over Binary method (Hosseinali and Alesheikh 2008). Here, lithological units, geophysical data, mineralization, faults and other structures, and alterations form the layers. Integrating information layers was done in Arc GIS 9.3 software, and mineral potential map was provided. Then in order to achieve more reasonable results, pixels value of mineral potential raster maps was extracted and C-A fractal modeling carried out on them, and mineral potential map was modified. Finally, to measure validity, the results were compared with stream sediments geochemical anomalies of copper and gold provided by C-A fractal modeling, and also the information derived from field observations.

1. Geological setting

The saveh 1:100,000 sheet is located in Urumieh-Dokhtar magmatic belt, oriented NW-SE (Fig. 1), which is the main host for porphyry and epithermal metallic deposits especially for Cu, Au and Mo (Afzal et al. 2010; Berberian and King 1981; Dargahi et al. 2010; Shahabpour 1994).

As depicted in Fig. 1, all outcrops of the region related to Cenozoic and older rocks in the surveyed area do not have outcropping. Most of outcrops are related to upper-mid Eocene volcanic units, which have covered mostly the part of Saveh sheet and generally are volcanic with sedimentary intercalations (Saeedi et al. eds. 2013). The most significant volcanic activity has occurred in Eocene which has resulted in the formation of the andesite, trachyte, trachyandesite, rhyolite, rhyo-dacite, ignimbrite and acidic tuffs. Iintrusive rocks (granite, granodiorite, tonalite, diorite) and great displacement by breccia-pressure faulting have completely disrupted these units (Rezaei-Kahkhaei et al. 2011). Neogene and Quaternary sedimentary units consisting of sandstone deposits, conglomerate, nummulite bearing limestone have also considerable spread in this region. According to the carried out studies,

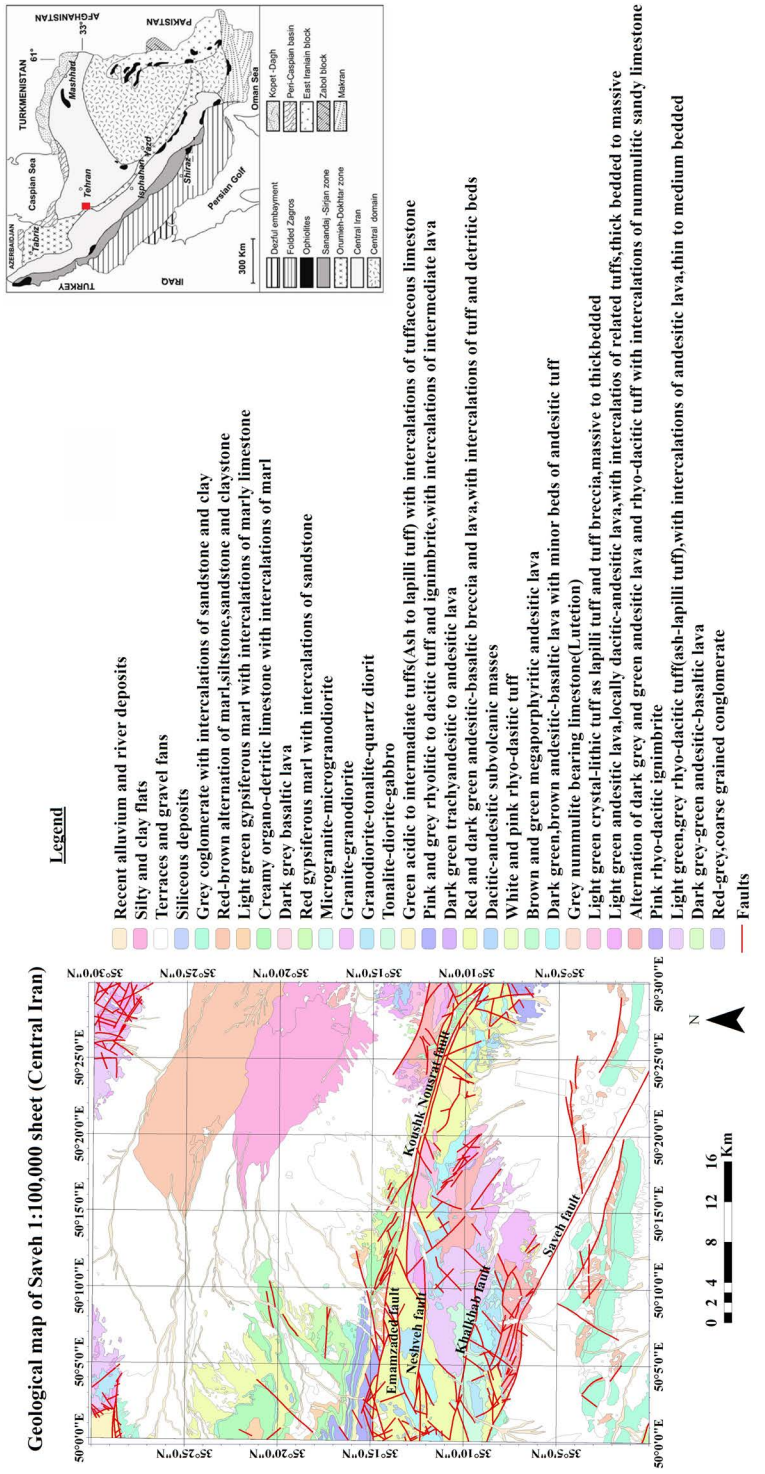

Fig. 1. Location of the Saveh 1 : 100,000 sheet in structural map of Iran and its geological map (Ghalamghash et al. 1998)

Rys. 1. Położenie obszaru Saveh na mapie Iranu w skali 1: 100 000 oraz mapa geologiczna tego rejonu (Ghalamghash et al. 1998)

magmatism in Urumieh-Dokhtar magmatic belt originally had tholeiitic nature, in the course of time it is transmuted to calc-alkaline and eventually to alkaline, but lithogeochemical data though tentatively, shows that this set generally has calc-alkaline composition which is the result of gabbroic magmatic differentiation and synchronous impregnation between the mentioned magma and a rhyolitic magma. Existent structures in region have WNW-ESE trend (Saeedi et al. eds. 2013).

2. Methods

2.1. Index overlay

In prospection of different ore deposits, numerous maps with unique characteristics are gathered, prepared, processed and integrated on technical principles by experienced experts, then mineral potential map is produced (Bonnefoy et al. 2002). There are various integration models categorized by kind of functions and their executive routine: Knowledge driven or Data driven. Knowledge driven: Expert experience and scientific knowledge are used for executing models. Data driven: Models are based on existent solutions and dependency value computation (Bonham-Carter 1994; Pazand et al. 2014; Porwal et al. 2003). Many researchers (Carranza et al. 1999; Cassard et al. 2008; Chico-Olmo et al. 2002; Feltrin 2008; Hariri 2003; Partington 2010) have used data-driven and knowledge-driven approaches in generating proper maps for prospection of ore deposits.

Index overlay method is a geographic information system operation and because of that layers have association by a common region, based on occupied space (Bonham-Carter 1994). Generating compound maps by integrating various dataset in which every layer has disparate classes and importance in mineralization, is valued and weighted on the basis of knowledge-driven approach (Karimi and Valadan Zoej 2004). Then the average score of given weights is determined by the following equation (Bonham-Carter 1994):

$$\overline{S} = \frac{\sum_{i}^{n} S_{ij} W_i}{\sum_{i}^{n} W_i} \tag{1}$$

where $\overline{S}$ represents the average score for features (polygon, pixel), W_i represents the weight of i^{th} input map, S_{ij} indicates the score of j^{th} class from i^{th} map. The value of j is dependent on the class which really is present in current position.

2.2. C-A fractal model

This model proposed by Cheng et al. (1994) is utilized for expressing the relation between obtained results and geological, geochemical and mineralogical data. Easy application and ability for quantitative calculation of threshold values are the paramount specialties of this model which is based on the amount of area each specific concentration has occupied in the studied area for separation of geochemical anomalies from background. This model is depicted as follows (Afzal et al. 2010; Shamseddin Meigoony et al. 2014):

$$A(\rho \le \vartheta) \infty \rho^{-a_1} \; ; A(\rho \ge \vartheta) \infty \rho^{-a_2} \tag{2}$$

In which $A(\rho)$ indicates area with higher concentration value than ρ level, ϑ represents threshold values and a_1 and a_2 are fractal dimensions. $A(\rho)$ is an area for a given ρ, equals the area of cells with higher concentration value than ρ multiplied by the number of cells.

In this model, the log-log plot of the assemblage frequency of number of areas versus concentration is drawn. By fitting straight lines to a series of points and obtaining break points of these lines, threshold values for target parameter are determined.

3. Presentation of information layers

3.1. Rock units layer

The studied area which is a part of Urumieh-Dokhtar magmatic belt, comprises subvolcanic, intrusives (granodiorite, tonalite and quartzdiorite) and acidic volcanic-subvolcanic rocks including rhyolitic, dacitic, trachyandesitic lava and andesite (Ghalamghash et al. 1998; Rezaei-Kahkhaei et al. 2011). Accordingly, lithological units relevant to mineralization in Saveh 1:100,000 sheet were surveyed. Considering the effect and significance of these units, after digitizing the geological map, in classification of rock units, suitable weight was given to them (Table 1) and its geological map is shown in Fig. 2a.

3.2. Geophysical layer

To interpret airborne magnetic data (with 7.5 km taken line distance) at first, the total intensity map of magnetic field was prepared and the effect of international geomagnetic reference field (IGRF) dependent upon geogravity field was calculated and omitted from observed magnetic data (total intensity of magnetic field: Almasi et al. 2014; Filho et al. 2007; Silva et al. 2003). Then implementing reduction to the pole applied as the base of other

Table 1. Weighting rock units

Tabela 1. Przypisanie odpowiednich wag skałom

Rock units	Weight
Granodiorite-tonalite-quartzdiorite	20
Microgranite-microgranodiorite-granite-granodiorite	19
Tonalite-diorite-gabbro	18
Trachyandesite to andesite lava	17
Megaporphyritic andesitic lava	16
Rhyo-dacitic tuff (ash-lapilli tuff) with intercalations of andesitic lava	15
Andesitic lava, locally dacitic-andesitic	14
Basaltic lava	13
Dacitic-andesitic subvolcanic masses	12
Rhyo-dacitic ignimbrite	11
Rhyolitic to dacitic tuff and ignimbrite with intercalations of intermediate lava	10
Andesitic- basaltic lava with beds of andesitic tiff	9
Andesitic-basaltic breccia and lava with intercalations of tuff and detritic beds	8
Rhyo-dacitic tuffs	7
Crystal-lithic tuff as lapilli tuff and tuff breccia massive to thickbedded	6
Acidic to intermediate tuffs (ash to lapilli tuff) with intercalations of tuffaceous limestone and thin bedded tuff	5
Nummulite bearing limestone and alternation of andesitic lava and rhyo-dacitic tuff with intercalations of nummulitic sandy limestone	2
Conglomerate and sandstone and coarse grained conglomerate, conglomerate with intercalations of sandstone and conglomerate and sandstone	1
Gypsiferous marl and limestone with intercalations of marl and alternation of siltstone and conglomerate	1
Recent alluvium and river deposits and silty and clayey flats, terraces and travertine	1

filters and first vertical derivative, data were analyzed. In the end shallow magnetic bodies were extracted (Fig. 2b).

3.3. Mineralization

In Saveh 1:100,000 sheet, as shown in Fig. 2c, ore indications are restricted to some barite, copper, iron and silica mines. Mineralization can be divided into two parts: copper and

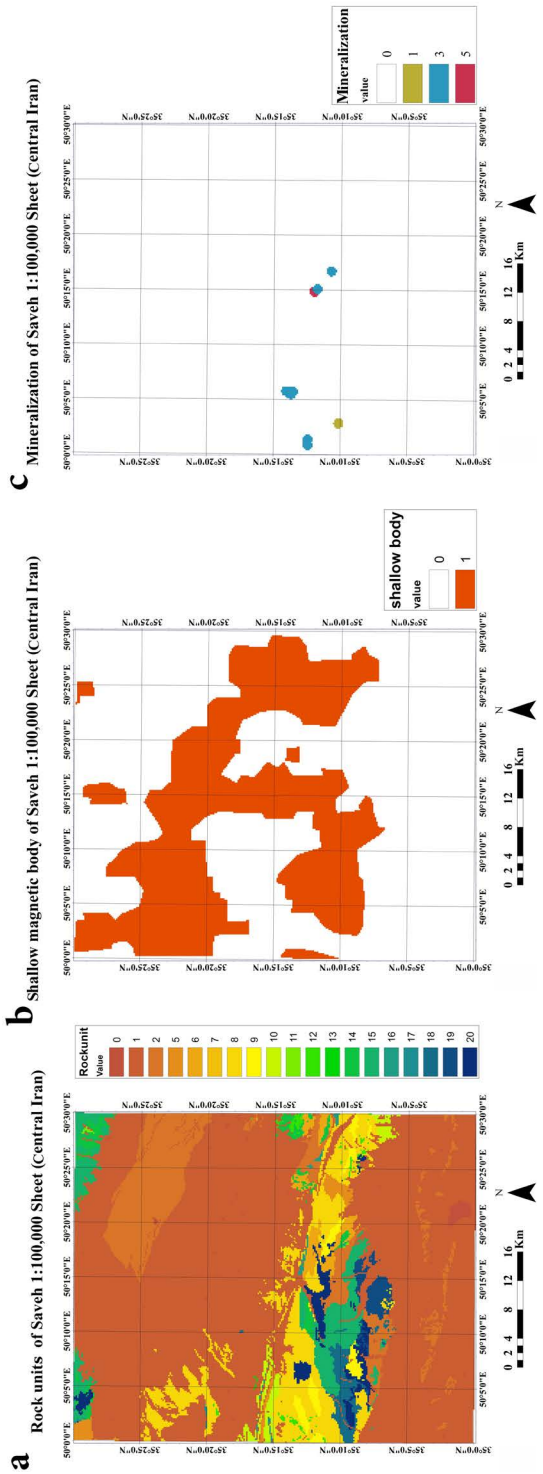

Fig. 2. Raster maps of a) rock units layer (explanations to colors and values have been provided in Table 1);
b) geophysical shallow magnetic bodies layer;
c) mineralization layer (explanations have been provided in Table 2)

Rys. 2. Mapy rastrowe
a – warstwy skalne (wyjaśnienia kolorów i wartości zostały przedstawione w tabeli 1),
b – płytkie geofizyczne anomalie od zaburzających obiektów magnetycznych (anomalie magnetyczne),
c – warstwy mineralizacji (wyjaśnienia zostały przedstawione w tabeli 2)

iron mineralization in siliceous vein and veinlet in center and west region, copper and iron mineralization in basaltic-basaltic andesite unit in the west of the studied area in Paighambar Shmouil region (Ghalamghash et al. 1998; Saeedi et al. eds. 2013). With regard to the importance of ore mineral type, each was given a suitable weight score (Table 2).

Table 2. Weighting and buffering of mineralization layer

Tabela 2. Przypisanie wag badanym warstwom

Mineralization	Weight	Buffer [m]
Copper	5	700
Copper, Iron	3	700
Copper, Silica	1	700

3.4. Faults and other structures

For preparing the layer related to faults and other structures, Saveh geological map, ETM^+ and airborne geophysical data were used. Generally, existent structures in the area have NW-SE trend. Regarding the dominant displacement pattern on the area (breccia-pressure) regional faults, in most cases have both horizontal and vertical displacement components (Ghalamghash et al. 1998; Saeedi et al. eds. 2013). According to the geological map of Saveh, the most important faults are Koushk Nousrat, Khalkhab and Saveh (Fig. 1). Association of mentioned faults and shallow magnetic bodies in geophysical data is noticeable. Concerning the importance and role of faults in mineral concentration, the survey of faults' relation with mineralization and also the study of suitable locations for settlement of Cu and Au mineralization are considered significant. Geological faults were buffered at the rate of 300 m based on optimal distance between the faults and the nearest mineral indexes, then with respect to their significance and role were valued (Carranza 2002; Table 3 and Fig. 3a).

Table 3. Weighting of faults presented on geological map

Tabela 3. Przypisanie wag do uskoków przedstawionych na mapie geologicznej

Geological fault	Weight
Major and minor faults	5
Thrust faults	4
Oblique slip faults	3
Strike slip faults	2
Inferred faults	1

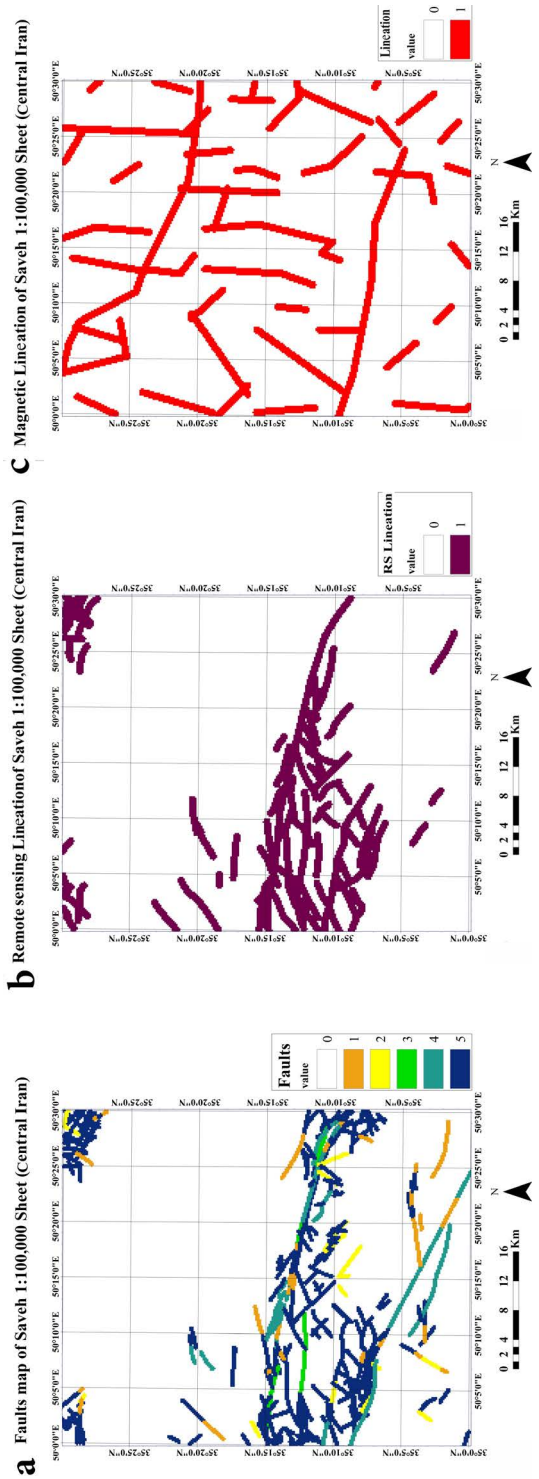

Fig. 3. Raster map layers of a) faults, geological map, colors refer to weight; b) remote sensing lineations; c) geophysical magnetic lineations

Rys. 3. Mapa rastrowa warstw

a – uskoki, dane geologiczne (kolory odpowiadają przyjętym wagom), b – lineamenty wyznaczone teledekcyjnie, c – lineamenty wyznaczone metodą magnetyczną

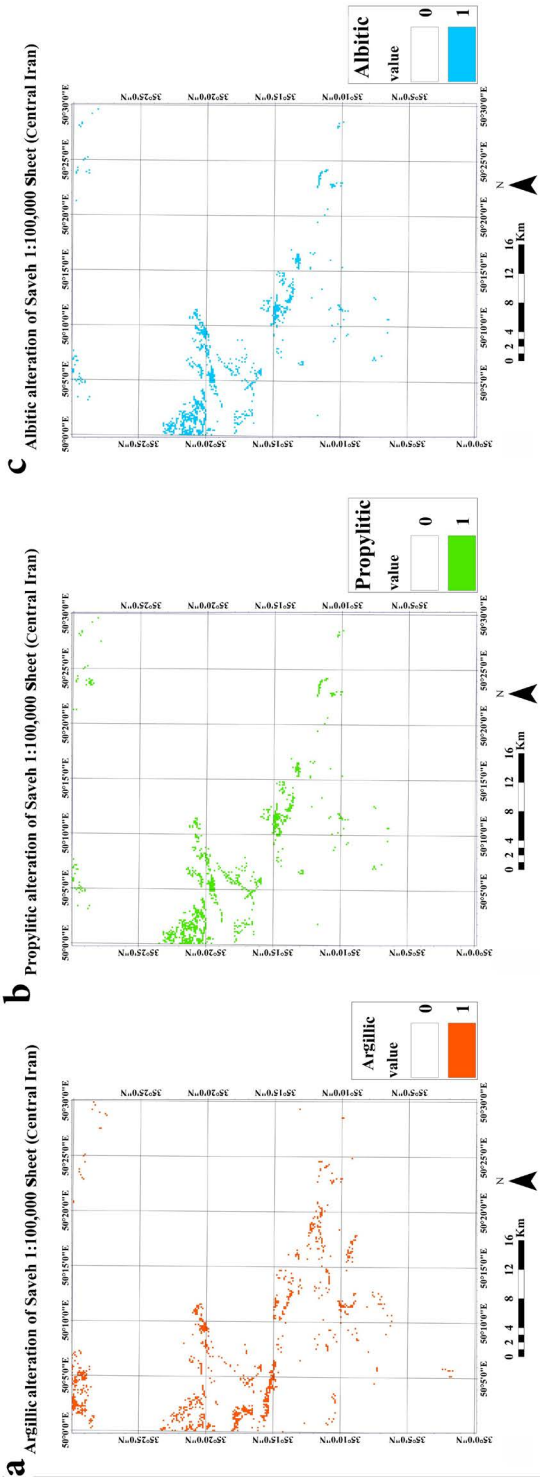

Fig. 4. Raster maps of a) argillic alteration layer; b) propylitic alteration layer; c) albitic alteration layer

Rys. 4. Mapy rastrowa

a – warstwa zmian argilitowych, b – warstwa zmian propylitowych, c – warstwa albitowa

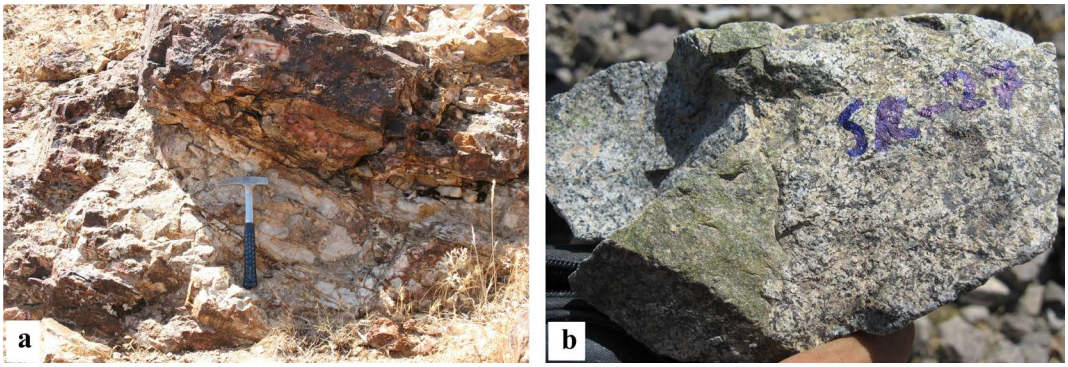

Fig. 5. a) Argillic alteration with iron hydroxide impregnation resulted from disintegration of pyrite grains, b) macroscopic sample of gabbro-diorite with epidotized xenolith as an indicator of propylitic alteration in Saveh 1:100,000 sheet

Rys. 5. a) zmiany argilitowe impregnowane wodorotlenkiem żelaza w wyniku dezintegracji ziarn pirytu, b) makroskopowa próbka gabro-dioryt z epidotyzowanym ksenolitem jako wskaźnik zmian propylitowych w Saveh, skala 1: 100.000

Also, surface structures were extracted using ETM^+ multi-spectral data with visual interpretation (RGB: 531) which their general trend corresponds with geological faults trend. Structures were buffered at the rate of 500m and then valued (Fig. 3b). Then deep structures were surveyed by the performed aeromagnetic data which were buffered at the rate of 500 m (Fig. 3c).

3.5. Alteration layer

In order to identify and separate alteration zones, the ASTER multi-spectral data were processed. In this study, using matched filtering (MF) and integrating it with regional geological map, argillic, propylitic and albitic alterations were recognized. It revealed that these alteration zones have been mostly assembled in a region in which a large granodiorite mass have intruded into Eocene basalt-andesite lava and volcanic breccia and caused the alteration. Argillic alteration is observed in NE regions around rhyodacitic tuff with intercalations of andesite lava, in NW around granodiorite-tonalite-quartzdiorite, in center, with a NW-SE trend conformed to dacitic, andesitic, tonalite-diorite, gabrro, subvolcanics and rhyo-dacitic tuffs with intercalations of andesite lava and volcanic breccia and basaltic-andesite lava with intercalations of tuff and brecciated layers (Figs 4a, 5a).

Propylitic alteration is also observed in west and central parts of the area, conformed to volcanic breccia and basaltic-andesitic lava with intercalations of tuff and around tonalite-granodiorite, quartzdiorite and dacite intrusives. Propylitic alteration with epidote and chlorite is mainly formed in basic and diorite-gabbro rocks which have been influenced by hydrothermal fluids (Figs 4b, 5b). Albitic alteration mostly exists in the central parts with a NW-SE trend conformed to Oligocene granitoid intrusives (Fig. 4c).

4. Integrating information layers

After preparing and processing information layers and classifying them, each of the information layers was given specific score due to the metallogenic nature of region and based on the importance of different layers for Au and Cu prospects (Table 4). After the examination of promising areas results, it was determined that dark blue areas in center, west and also parts of NE and NW of region, take the highest priority. These regions are conformed to Oligocene granite, granodiorite, tonalite and Eocene subvolcanics and connected with fault system. Light blue areas in west and SE of region, take subsequent priority which mostly are connected with andesitic lavas of dacite-andesite composition (Fig. 6).

Table 4. Scoring of different exploration layers

Tabela 4. Punktacja różnych badanych warstw

Exploration data		Score
Rock units		0.6
Shallow magnetic bodies		0.2
Mineralization		0.25
Faults and structures	Geological	0.3
	Geophysical	0.35
	Remote sensing	0.15
Alterations	Propylitic	0.4
	Argillic	0.5
	Albitic	0.45

5. Fractal modeling

After obtaining the results of integrating information layers, pixels value of gained map were extracted. Applying C-A fractal model, threshold values were determined with respect to Fig. 7 and the results are shown in Table 5. Then applying these threshold values to first integration map, important areas were prioritized. Promising areas in a small-scale and with high exploration priority in center, west and also parts of NW of region, are conformed to granodiorite intrusives and connected with fault structures. Next priority in center, west, NE and NW are conformed to granite, diorite, and also subvolcanic units respectively (Fig. 8).

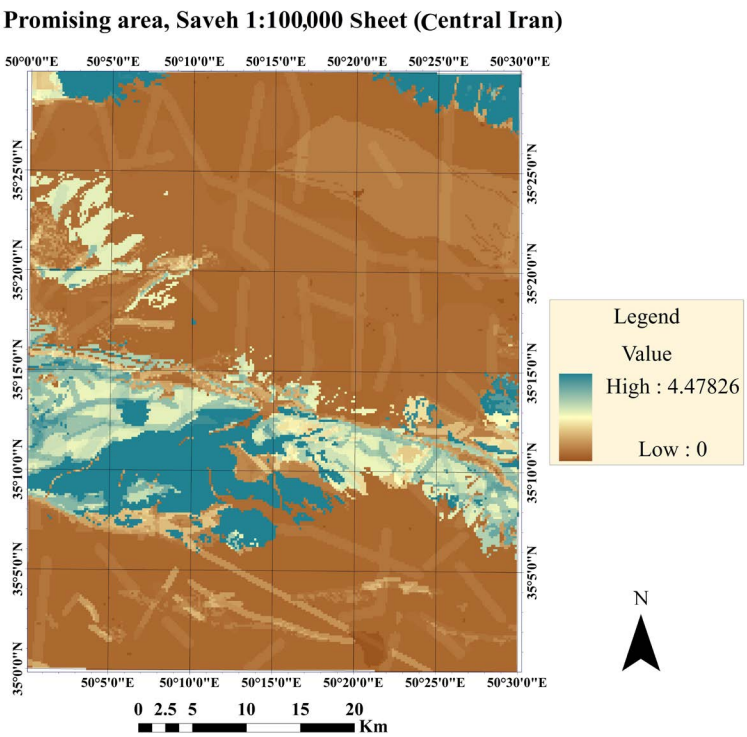

Fig. 6. Mineral potential map resulted from integration of information layers in Saveh 1:100,000 sheet

Rys. 6. Mapa przypuszczalnej mineralizacji opracowanej na podstawie złożenia (integracji) informacji warstwowej w Saveh, skala 1: 100.000

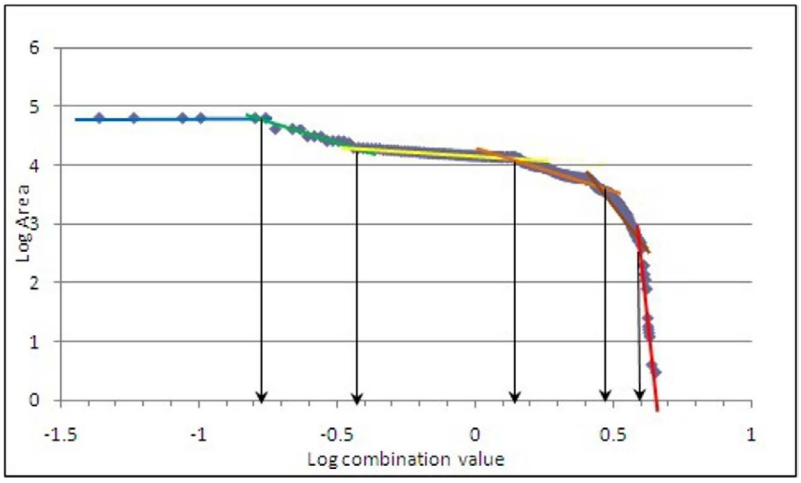

Fig. 7. Log-log plot of C-A fractal model

Rys. 7. Wykres log-log modelu fraktalnego C-A

Table 5. Calculated threshold values for pixels value

Tabela 5. Obliczone wartości progowe dla pikseli

Threshold	Very low intensity threshold	Low intensity threshold	Moderate intensity threshold	High intensity threshold	Very high intensity threshold	Extremely high intensity threshold
	0.162	0.363	1.348	2.951	3.981	4.478

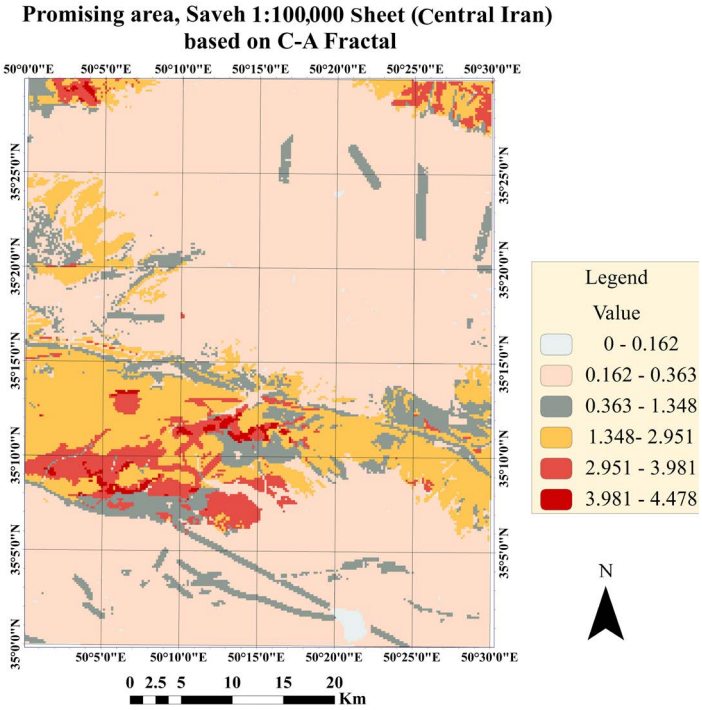

Fig. 8. Exploration priority map of C-A fractal modeling of integrated information layers in Saveh 1:100,000 sheet

Rys. 8. Mapa perspektywicznych poszukiwań (eksploracji) opracowana na podstawie modelu fraktalnego C-A wynikającego ze zintegrowanej informacji warstwowej w Saveh, skala 1:100 000

6. Field observation and validation the results

To assess the accuracy of the results, mineral resources potential map was compared with the geochemical maps of copper and gold based on stream sediments data (Fig. 9). In these maps, C-A fractal model has been used for determination of threshold values and separation of anomaly from background in which the anomalous threshold values for copper and

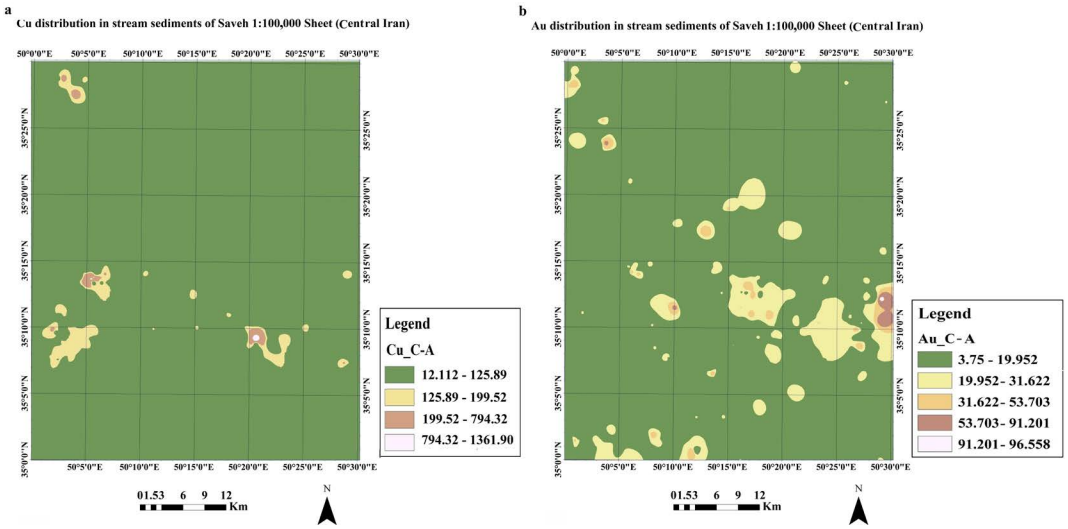

Fig. 9. Geochemical maps of Saveh 1:100,000 sheet based on stream sediments data
a) copper, b) gold

Rys. 9. Mapy geochemiczne obszaru Saveh (skala 1: 100 000)
opracowane na podstawie danych sedymentologicznych
a) miedź, b) złoto

gold are 199.52 and 53.703 respectively. On this basis, it can be observed that geochemical anomalies of copper in SE and limitedly in west and NW, and geochemical anomalies of gold in east and, limitedly, in center and NW of region correspond with the main priorities of the mineral map. According to field observations Eocene andesite, latite andesite, tuff and pyroclastics have been also influenced by granitoid postmagmatic fluid, and led to pyrite, chalcopyrite and bornite mineralization with malachite impregnation (Fig. 10a). Because of weathering and meteoric waters, pyrite has deteriorated and changed into iron hydroxide

Fig. 10. Macroscopic samples in Saveh 1:100,000 sheet
a) oxidized chalcopyrite, b) malachite, c) vuggy quartz with malachite impregnation

Rys. 10. Makroskopowe próbki pochodzące z obszaru Saveh, skala 1: 100 000
a) utleniony chalkopiryt, b) malachit, c) porowaty kwarc impregnowany malachitem

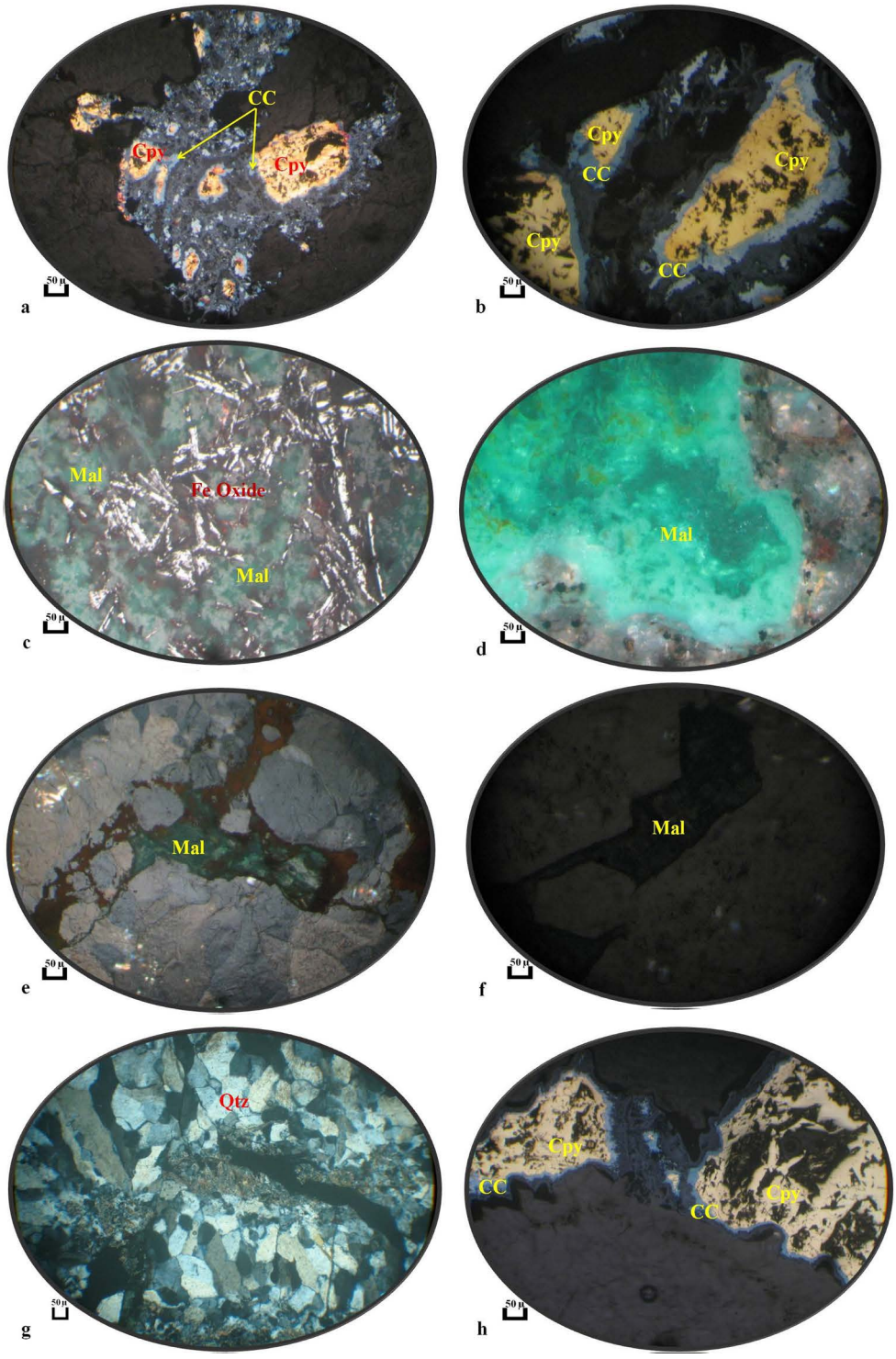
CC
Cpy
Cpy
50 µ
a
Cpy
CC
Cpy
Cpy
CC
50 µ
b
Mal
Fe Oxide
Mal
50 µ
c
Mal
50 µ
d
Mal
50 µ
e
Mal
50 µ
f
Qtz
50 µ
g
Cpy
CC
Cpy
CC
50 µ
h

Table 6. Results of ICP-MS analysis in Saveh 1:100,000 sheet

Tabela 6. Wyniki analizy ICP-MS w Saveh, skala 1:100 000

Sample code	Cu (ppm)	Au (ppb)
Sa1	66 769.6	389.6744
Sa2	52 839.4	29.54519
Sa3	50 299.2	1 134
Sa4	45 134.4	136.836
Sa5	13 095	1 499
Sa6	8 671	0.01
Sa7	2 580.47	100
Sa8	1 669.17	152
Sa9	1 103.05	1 575
Sa10	1 071.86	86

Fig. 11. Images of microscopic polished thin sections of Saveh 1:100,000 sheet samples
a, b) image of chalcopyrite disintegration and emergence of remnant texture so that remnants of chalcopyrite have been encompassed by chalcocite (PPL, 20 × 10X);
c, d) image of acicular-formed blades of hematite in rock matrix which have crossed each other and among them malachite has been settled as secondary product (turquoise). This malachite is a product of chalcopyrite disintegration (PPL, 20 × 10X);
e, f) fractures occurred inside quartz have resulted in entering mineral phase in it and then disintegrating by weathering and settling secondary products such as malachite in microcracks. Malachite as secondary product of chalcopyrite disintegration (PPL, 20 × 10X);
g) image of segmentation of quartz vein by sericitization phase and occuring copper mineralization with sericitization phase (XPL, 20 × 10X);
h) mineralized phase which is seen with phyllic alteration or sericitization, chalcopyrite is observed in the form of vein – a veinlet with sericitic veins; this phase later affected by weathering and also meteoric waters have been disintegrated and changed to chalcocite (PPL, 20 × 10X)
Qtz – Quartz, Cpy – Chalcopyrite, Cc – Chalcocite, Mal – Malachite, Fe Oxide – Hematite

Rys. 11. Obrazy mikroskopowe wypolerowanych próbek z obszaru Saveh, skala1: 100 000
a, b − obraz dezintegracji chalkopirytu zawierający resztki struktury chalkopirytu z wtrąceniami chalkozynu (PPL, 20 × 10X), c, d − obraz igiełkowy kryształu hematytu w tle skalnym i dodatkowo występującym wtórnym malachitem. Ten malachit jest produktem rozkładu chalkopirytu (PPL, 20 × 10X), e, f – spękania występujące wewnątrz kwarcu, wytworzone w procesie mineralizacji i zdezintegrowane w procesie wietrzenia z osadzonymi wtórnymi produktami takimi jak malachit. Malachit jest wtórnym produktem rozpadu chalkopirytu (PPL, 20 × 10X), g − obraz podziału żyły kwarcowej rozpadu w fazie serycytyzacja z występującą mineralizacją i serycytyzacją miedzi (XPL, 20 × 10X), h − faza zmineralizowana ze zmianami fylitowymi lub serycytyzacji − chalkopiryt jest widoczny w postaci żyłek wraz z żyłkami serycytowymi; ta faza podlegała wpływowi wietrzenia oraz wód z opadów atmosferycznych, została zdezintegrowana i zmieniona do postaci chalkozynu (PPL, 20 × 10X)
QTZ – kwarc , CpY – chalkopiryt, DW – chalkozyn, Mal – Malachit, Fe Oxide – Hematyt

(goethite, lepidocrocite) and the effects of their brown color are thoroughly visible along the conjugate joints (Fig. 10b). Siliceous veins in the form of cryptocrystalline to dark gray fine grains and sometimes vuggy quartz usually with different amounts of sulfide and jaspery bands in some epithermal mineralized areas visible in outcrops (Fig. 10c).

To determine the physicochemical characteristics of mineral fluid, survey, and identify alteration types, sampling was done for mineralography and petrography, their polished thin sections were studied. The obtained results from the study of these sections showed that pyrite, chalcopyrite, bornite, chalcocite, covellite and galena mineralization usually exist

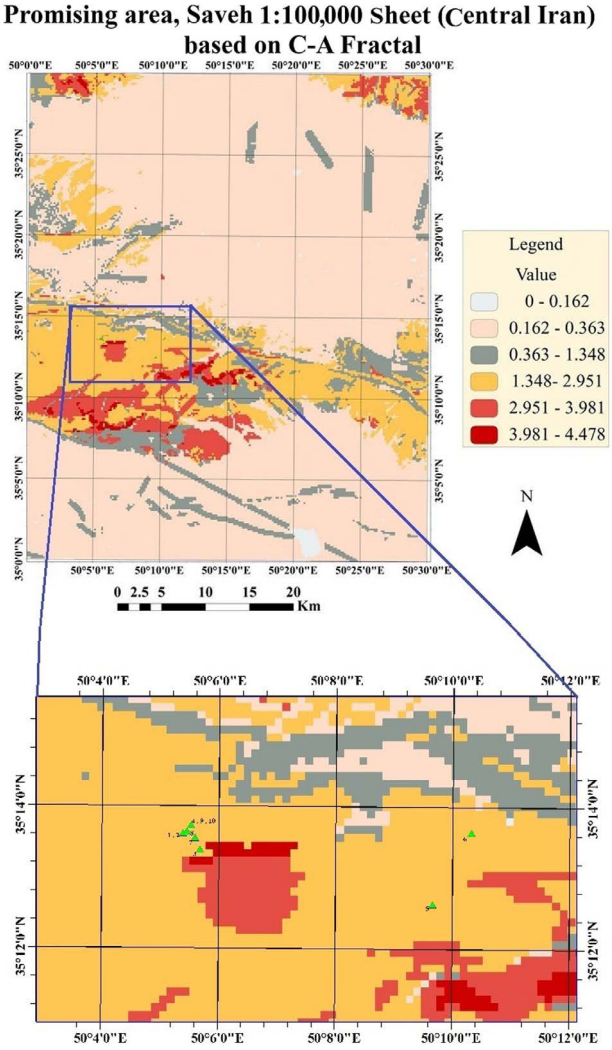

Fig. 12. Map of final exploration priorities with potential areas of field observation in Saveh 1:100,000 sheet

Rys. 12. Mapa z wytypowanymi priorytetowymi danymi do poszukiwań z zaznaczeniem perspektywicznych obszarów badań w Saveh, skala1: 100 000

with silica and barite vein-veinlet. Under the influence of chalcopyrite disintegration due to weathering, goethite, and malachite as secondary products are clearly observed marginally and along the fractures (Fig. 11). In order to determine indefinite mineral phases, samples were analyzed by XRD and ICP-MS methods; sampling location and their characteristics have been provided in Fig. 12 and Table 6 respectively. The XRD results signify that volcanic rocks of region have been exposed to regional argillic, phyllic, propylitic and siliceous hydrothermal alterations due to the ascend of late magmatic fluid.

Conclusion

Mineral potential map derived from the integration of different information layers, includes range of priorities in 0–4.47826 interval on which highly potential areas are situated in center region extending from west to east, and limitedly in NW and NE of the studied area. Carrying out fractal modeling on this map, the results of the first map were prioritized. Comparing the obtained results with geochemical anomaly maps and also by accomplished field observations in region, microscopic sections studies and performed analyses, highly priority regions were specified. These regions contain pyrite, chalcopyrite and galena mineralization, resulted from postmagmatic fluid; at places, due to oxidation processes, other secondary products such as hematite, goethite, and in some regions malachite impregnation are clearly observable. Also ICP-MS analysis of taken samples proves Cu and Au mineralization in these regions. Thus we can conclude that carrying out fractal modeling while prioritizing different regions by calculation of threshold values for priorities based on fractal nature of data, results in optimizing of the determined potential areas.

REFERENCES

Afzal et al. 2010 – Afzal, P., Khakzad, A., Moarefvand, P., Rashidnejad Omran, N., Esfandiari, B. and Fadakar Alghalandis, Y. 2010. Geochemical anomaly separation by multifractal modeling in Kahang (GorGor) porphyry system. Central Iran. *Journal of Geochemical Exploration* 104, pp. 34–46.

Afzal et al. 2012 – Afzal, P., Fadakar Alghalandis, Y., Moarefvand, P., Rashidnejad Omran, N. and Asadi Haroni, H. 2012. Application of power-spectrum-volume fractal method for detecting hypogene, supergene enrichment, leached and barren zones in Kahang Cu porphyry deposit, Central Iran. *Journal of Geochemical Exploration* 112, pp. 131–138.

Afzal et al. 2013 – Afzal, P., Dadashzadeh Ahari, H., Rashidnejad Omran, N. and Aliyari, F. 2013. Delineation of gold mineralized zones using concentration–volume fractal model in Qolqoleh gold deposit, NW Iran. *Ore Geology Review* 55, pp. 125–133.

Afzal et al. 2014 – Afzal, P., Alhoseini, S.H., Tokhmechi, B., Kaveh Ahangaran, D., Yasrebi, A.B., Madani, N. and Wetherelt, A. 2014. Outlining of high quality coking coal by concentration–volume fractal model and turning bands simulation in East-Parvadeh coal deposit, Central Iran. *International Journal of Coal Geology* 127, pp. 88–99.

Agterberg, F.P. 1995. Multifractal modeling of the sizes and grades of giant and supergiant deposits. *International Geology Review* 37, pp. 1–8.

Almasi et al. 2014 – Almasi, A., Jafarirad, A., Kheyrollahi, H., Rahimi, M. and Afzal, P. 2014. Evaluation of structural and geological factors in orogenic gold type mineralization using airborne geophysical data, Kervian area, NW of Iran. *Exploration Geophysicists* doi:10.1071/EG13053.

Berberian, M. and King, G.C. 1981. Towards a paleogeography and tectonic evolution of Iran. *Canadian Journal of Earth Sciences* 18, pp. 210–265.

Bonham-Carter, G.F. 1991. *Geographic Information System for Geoscientists: Modeling with GIS*. Ontario: Pergamon press, 470 pp.

Bonham-Carter, G.F. 1994. *Geographic Information Systems for Geoscientists: Modelling with GIS*. Oxford: Pergamon Press, 398 pp.

Bonnefoy et al. 2002 – Bonnefoy, D., Braux, C., Corpel, G., Delpont, G. and Weber, C. 2002. Combined interpretation of remote sensing imagery and geophysical data: exploration for gold in southern Brittany, France. *Advances in Space Research* 12(7), pp. 17-25.

Carranza et al. 1999 – Carranza, E.J.M., Mangaoang, J.C. and Haleh, M. 1999. Application of mineral exploration models and GIS to generate mineral potential maps as input for optimum land-use planning in the Philippines. *Natural Resources Research* 2(8), pp. 165–173.

Carranza, E.J.M. 2002. Geologically-constrained mineral potential mapping. *Ph.D thesis,* ITC Delft, Netherlands, pp. 1–474.

Carranza, E.J.M. 2008. *Geochemical anomaly and mineral prospectivity mapping in GIS*. Amsterdam: Elsevier, 368 pp.

Cassard et al. 2008 – Cassard, C., Billa, M., Lambert, A., Picot, J., Husson, Y., Lasserre, L. and Delor, C. 2008. Gold predictivity mapping in French Guiana using an expert-guided data-driven approach based on a regional-scale GIS. *Ore Geology Reviews* 34, pp. 471–500.

Cheng et al. 1994 – Cheng, Q., Agterberg, F.P.and Ballantyne, S.B. 1994. The separation of geochemical anomalies from background by fractal methods. *Journal of Geochemical Exploration* 51, pp. 109–130.

Cheng, Q. 1999. Spatial and scaling modelling for geochemical anomaly separation. *Journal of Geochemical Exploration* 65(3), pp. 175–194.

Cheng, Q. and Agterberg, F.P. 2009. Singularity analysis of ore-mineral and toxic trace elements in stream sediments. *Computers & Geosciences* 35(2), pp. 234–244.

Chico-Olmo et al. 2002 – Chico-Olmo, M., Abarca, F. and Rigol, J.P. 2002. Development of a decision support system based on remote sensing and GIS techniques for gold-rich area identification in SE Spain. *International Journal of Remote Sensing* 232, pp. 4801–4814.

Dargahi et al. 2010 – Dargahi, S., Arvin, M., Pan, Y. and Babaei, A. 2010. Petrogenesis of Post-Collisional A-type granitoid from the Urumieh-Dokhtar magmatic assemblage, Southwestern Kerman, Iran: constraints on the Arabian-Eurasian continental collision. *Lithos* 115, pp. 190–204.

Davis J.C. 2002. *Statistics and data analysis in Geology.* New York: John Wiley and Sons Inc, 638 pp.

Feltrin, L. 2008. Predictive modeling of prospectivity for Pb–Zn deposits in the Lawn Hill Region, Queensland, Australia. *Ore Geology Reviews* 34, pp. 399–427.

Filho et al. 2007 – Filho, C.R.S., Nunes, A.R., Leite, E.P., Monteiro, L.V.S. and Xavier, R.P. 2007. Spatial Analysis of Airborne Geophysical Data Applied to Geological Mapping and Mineral Prospecting in the Serra Leste Region, Caraja´s Mineral Province, Brazil. *Surveys in Geophysics* 28, pp. 377–405.

Ghalamghash et al. 1998 – Ghalamghash, J., Fonoudi, M. and Mehrpartou, M. eds. 1998. *Geological map of Saveh 1:100,000 sheet*. Tehran: Geological Survey of Iran.

Hariri, M. 2003. Use of GIS (geographic information system) in determining relationship between geology, structure and mineral prospects, southern part of the Arabian Shield, Saudi Arabia, Pakistan. *Journal of Applied Sciences* 3(2), pp. 92–96.

Harris, J.R. 1989. Data integration for gold exploration in eastern Nova Scotia using a GIS. *Remote Sensing for Exploration Geology*. Calgary, Alberta, pp. 233–249.

Hosseinali, F. and Alesheikh, A. 2008. Weighting Spatial Information in GIS for Copper Mining Exploration. *American Journal of Applied Sciences* pp. 1187–1198.

Karimi, M. and Valadan Zoej, M.J. 2004. Mineral potential mapping of copper minerals with GIS. *Geo-Imagery Bridging Continents, XXth ISPRS Congress.* Istanbul, 12-23 July, 2004. pp. 1103–1108.

Li et al. 2003 – Li, C.J., Ma, T.H. and Shi, J.F. 2003. Application of a fractal method relating concentration and distances for separation of geochemical anomalie from background. *Journal of Geochemical Exploration* 77, pp. 167–175.

Malczewski, J. 2006. Ordered weighted averaging with fuzzy quantifi ers: GIS-based multicriteria evaluation for land-use suitability analysis. *International Journal of Applied Earth Observation and Geo information* 8(4), pp. 270–277.

Mandelbrot, B.B. 1983. *The fractal geometry of Nature.* San Fransisco: W.H. Freeman, 468 pp.

Moradi et al. 2014 – Moradi, M., Basiri, S., Kananian, A. and Kabiri, K. 2014. Fuzzy logic modeling for hydrothermal gold mineralization mapping using geochemical, geological, ASTER imageries and other geo-data, a case study in Central Alborz, Iran. *Earth science informatics* doi:10.1007/s12145-014-0151-9.

Noorollahi et al. 2008 – Noorollahi,Y., Itoi, R., Fujii, H. and Tanaka, T. 2008. GIS integration model for geothermal exploration and well siting. *Geothermics* 37, pp.107–131.

Partington, G. 2010. Developing models using GIS to assess geological and economic risk: an example from VMS copper gold mineral exploration in Oman. *Ore Geology Reviews* 38, pp. 197–207.

Pazand et al. 2011 – Pazand, K., Hezarkhani, A., Ataei, M. and Ghanbari, Y. 2011. Combining AHP with GIS for predictive Cu porphyry potential mapping: a case study in Ahar Area (NW, Iran). *Natural Resources Research* 20(4), pp. 251–262.

Pazand et al. 2014 – Pazand, K., Hezarkhani, A. and Ghanbari, Y. 2014. Fuzzy analytical hierarchy process and GIS for predictive Cu porphyry potential mapping: a case study in Ahar–Arasbaran Zone (NW, Iran). *Arabian Journal of Geosciences* 7, pp. 241–251.

Porwal et al. 2003 – Porwal, A., Carranza, E. and Hale, M. 2003. Knowledge-driven and Data-driven Fuzzy Models for Predictive Mineral Potential Mapping. *Natural Resources Research* 12(1), pp. 1–25.

Porwal et al. 2006 – Porwal, A., Carranza, E.J.M. and Hale, M. 2006. A Hybrid Fuzzy Weights-of-Evidence Model for Mineral Potential Mapping. *Natural Resources Research* 15, pp. 1–14.

Rezaei Kahkhaei et al. 2011 – Rezaei Kahkhaei, M., Galindo, C., Pankhurst, R.J. and Esmaeily, D. 2011. Magmatic differentiation in the calc-alkaline Khalkhab–Neshveh pluton, Central Iran. *Journal of Asian Earth Sciences* 42, pp. 499–514.

Saeedi et al. 2013 – Saeedi, A., Maqsoudi, A. and Younesi, S. eds. 2013. *Geochemical Exploration in Saveh 1:100,000 Sheet*. Tehran: Geological Survey of Iran, 187 pp. *(in Persian)*.

Shahabpour, J. 1994. Post-mineral brecciadyke from the Sar-Cheshmehporphyry copper deposit, Kerman, Iran. *Exploration and Mining Geology journal* 3, pp. 39–43.

Shamseddin Meigoony et al. 2014 – Shamseddin Meigoony, M., Afzal, P., Gholinejad, M., Yasrebi, A.B. and Sadeghi, B. 2014. Delineation of geochemical anomalies using factor analysis and multifractal modeling based on stream sediments data in Sarajeh 1:100,000 sheet, Central Iran. *Arabian Journal of Geosciences* 7, pp. 5333–5343.

Silva et al. 2003 – Silva, A.M., Pires, A.C. and McCaffery, A. 2003. Application of airborne geophysical data to mineral exploration in the uneven exposed terrains of the Rio Das Velhas greenstone belt. *Revista Brasileira de Geociencias* 33, pp. 17–28.

Sim et al. 1999 – Sim, B.L., Agterberg, F.P. and Beaudry, C. 1999. Determining the cutoff between background and relative base metal contamination levels using multifractal methods. *Computers & Geosciences* 25, pp. 1023–1041.

Yousefifar et al. 2011 – Yousefifar, S., Khakzad, A., Asadi Harooni,H., Karami, J., Jafari, M.R. and Vosoughi Abedin, M. 2011. Prospecting of Au and Cu bearing targets by exploration data combination in southern part of dalli Cu-Au porphyry deposit, central iran. *Archives of Mining Sciences* 56(1), pp. 21–34.

Zuo, R. 2011. Identifying geochemical anomalies associated with Cu and Pb–Zn skarn mineralization using principal component analysis and spectrum–area fractal modeling in the Gangdese Belt, Tibet (China). *Journal of Geochemical Exploration* 111, pp. 13–22.

Zuo et al. 2009 – Zuo, R., Cheng, Q. and Xia, Q. 2009. Application of fractal models to characterization of vertical distribution of geochemical element concentration. *Journal of Geochemical Exploration* 102(1), pp. 37–43.

Zuo et al. 2013 – Zuo, R., Xia, Q. and Zhang,D.A. 2013. comparison study of the C–A and S–A models with singularity analysis to identify geochemical anomalies in covered areas. *Applied Geochemistry* 33, pp. 165–172.

PERSPEKTYWY POSZUKIWAŃ MIEDZI I ZŁOTA METODĄ WSKAŹNIKA INTEGRACJI I MODELOWANIA MULTIFRAKTALNEGO W SAVEH, SKALA 1:100 000, CENTRALNY IRAN

Słowa kluczowe

system informacji geograficznej (GIS), wskaźnik integracji, strefa złoża (C-A) model fraktali, pas magmowy Urumieh-Dokhtar, arkusz Saveh 1:100 000

Streszczenie

Badanie to ma na celu poszukiwanie miedzi i złota z perspektywicznych obszarów w Saveh na arkuszu 1:100 000, położonego w pasie magmowym w Urumieh-Dokhtar (Centralny Iran). System informacji geograficznej (GIS) jest skuteczny w rozpoznaniu przypuszczalnych zasobów surowców mineralnych poprzez gromadzenie, przetwarzanie warstwy ważenia poszukiwań i integracji map tematycznych. W celu uzyskania właściwych wyników dla potrzeb określenia potencjalnych obszarów do eksploatacji, użyto techniki modelowania i zintegrowanej informacji o warstwach geologicznych. W tym badaniu została użyta metoda wskaźnikowa, która jest kombinacją komputerowego sposobu przetwarzania danych i wiedzy eksperckiej. Badane warstwy geologiczne opisane są pojęciami litologicznymi, danymi geofizycznymi, stopniem mineralizacji oraz zaburzeniami tektonicznymi. Dla bardziej dokładnych badań, modelowanie fraktalne strefy złożowej (C-A) zostało przeprowadzone na podstawie zintegrowanych danych przedstawionych na mapie. Zastosowanie modelowania fraktalnego do tej mapy spowodowało poprawę jakości danych. W końcowej ocenie ważności obszarów prognostycznych, wyniki badań zostały porównane z wagami geochemicznymi anomalii z uwzględnieniem ukształtowania osadów , a także na podstawie obserwacji polowych. Obszary perspektywiczne o ograniczonym zasięgu występujące w centralnej i zachodniej części oraz w niektórych partiach części NW, zostały skorelowane z intruzjami granodiorytów; podobnie perspektywiczny obszar istnieje w części centralnej i zachodniej, NE i NW, który został skorelowany ze skałami granitowymi, diorytowymi i subwulkanicznymi. Dane te zostały również skorelowane z systemem uskoków. Wykonano badania: dyfrakcji rentgenowskiej (XRD), spektrometrii masowej (ICP-MS), jak również analizy mikroskopowe oraz pobrano właściwe próbki. Wszystkie badania wskazują na możliwość występowania epitermalnej mineralizacji pirytu, galeny, chalkopirytu wynikających z obecności płynów pomagmowych, a także produktów wtórnych, takich jak: hematyt, getyt i malachit powstałych jako rezultat procesów utleniania na tych obszarach

INVESTIGATION OF COPPER AND GOLD PROSPECTS USING INDEX OVERLAY INTEGRATION METHOD AND MULTIFRACTAL MODELING IN SAVEH 1:100,000 SHEET, CENTRAL IRAN

Keywords

geographic information system (GIS), index overlay integration method, concentration-area (C-A) fractal model, Urumieh-Dokhtar magmatic belt, Saveh 1:100,000 sheet

Abstract

This study aims at prospecting copper and gold promising areas in Saveh 1:100,000 sheet, situated in Urumieh-Dokhtar magmatic belt (Central Iran). Geographic information system (GIS) is effective in recognition of probable mineral resources by collecting, processing, exploration layer weighting and integrating thematic maps. As there is no certainty in different geological phenomena, modeling and integrating information layers are used to obtain suitable results for determining potential areas. In this study, index overlay method, which is a combination of software processing and expertise knowledge, was used. The survey layers consist of the lithologic units, geophysical data, mineralization, faults and structures and alteration. For more exact survey, concentration-area (C-A) fractal modeling was applied to the map of results obtained from integration. Applying fractal model to this map, the results of the original map were prioritized and became more limited. In the end for assessing the validity of determined promising areas, the results were compared with geochemical anomaly maps of stream sediments and also field observation was performed. Areas with high exploration priority with limited extend exist in center, west and some parts of NW, conformed to granodiorite intrusives and also next priority exists in center, west, NE and NW conformed to granite, diorite, and also subvolcanic rocks respectively. These prioroties are related to fault systems. In order to perform X-ray Diffraction (XRD), Inductively Coupled Plasma – Mass Sepctrometry (ICP-MS) analyses and microscopic studies, lithogeochemical samplings were done. All investigations indicate the possibility of pyrite, chalcopyrite and galena epithermal mineralizations resulted from post magmatic fluids, and also secondary products like hematite, goethite, and malachite as a result of oxidation processes in these areas.